JURNAL GEOGRAFI
Geografi dan Pengajarannya
ISSN : 1412 - 6982
e-ISSN : 2443-3977
Volume 24, Number 1, June 2026
https://journal.unesa.ac.id/index.php/jg
DOI : https://doi.org/10.26740/jggp.v24n1.p479-502

INTEGRATED REANALYSIS AND HIMAWARI-9 SATELLITE OBSERVATIONS OF WATERSPOUT FORMATION OVER THE BELIAH STRAIT (CASE STUDY: 17 JUNE 2025)

Reinal Taruna Wahyu Halawa[1], Yosafat Donni Haryanto[*]
[1]Meteorology Study Program, State College of Meteorology Climatology And Geophysics, Tangerang, Indonesia

ARTICLE INFO

Article history:
Received 26 Jan 2026
Revised 15 April 2026
Accepted 20 May 2026

***Keywords*:**
Waterspout, Mesoscale Convergence, Convective Instability, Himawari-9, Beliah Strait

ABSTRACT

This study investigates a waterspout event over the Beliah Strait, Indonesia, on 17 June 2025 between 11:30 and 13:00 WIB (04:30–06:00 UTC) using ERA5 reanalysis and Himawari-9 satellite observations. The event developed under weak synoptic forcing but was strongly influenced by mesoscale processes, including low-level wind convergence and intensifying boundary-layer vorticity. Time-height analysis revealed a deepening moist layer prior to convective development. Thermodynamic assessment from a Skew-T Log-P diagram indicated moderate atmospheric instability, with CAPE of 1204.3 J kg^{-1}, weak convective inhibition, a negative Lifted Index, and low LCL and LFC heights supporting rapid convection. Warm sea surface temperatures enhanced the low-level moisture supply over the narrow strait. Himawari-9 infrared imagery captured cloud-top cooling concurrent with peak convergence. The event was identified as a non-supercell waterspout associated with mesoscale convergence and favorable thermodynamic conditions.

A. INTRODUCTION

A waterspout, or whirlwind above the sea surface, is an extreme weather phenomenon similar to a tornado, except that it forms over water. This phenomenon can occur in both supercell and non-supercell storms. Although relatively small in size, waterspouts are still classified as mesoscale to microscale extreme weather events because they have strong rotating winds and a significant local impact (Chan et al., 2020; Chan et al., 2022; Renko et al., 2018). A number of observational and modeling studies show that the vertical circulation structure of waterspouts can resemble land tornadoes, with rotation intensifying up to several kilometers above sea level (Chan et al., 2020; Mihajlović et al., 2021). Therefore, waterspouts are considered dangerous to coastal infrastructure, small boats, fisheries, and maritime activities, making it essential to monitor them in early warning and disaster mitigation systems (Mihajlović et al., 2021; Renko et al., 2018).

[*]Correspondence address: yosafat.haryanto@stmkg.ac.id

In tropical regions, the combination of warm sea surface temperatures, high atmospheric humidity, and weather disturbances ranging from synoptic to mesoscale scales creates conditions that are highly conducive to the formation of deep convection and waterspouts (Mihajlović et al., 2021; Renko et al., 2018). Narrow bodies of water such as straits, bays, and estuaries, which are also busy shipping lanes, increase the risk of waterspouts, as they can interfere with navigational safety (Chan et al., 2022; Mihajlović et al., 2021). Climatological analysis also shows that waterspouts often appear in coastal or semi-enclosed sea areas, where the shape of the coastline, sea conditions, and local wind patterns increase convergence and vorticity in the lower atmosphere (Monterde et al., 2025; Mihajlović et al., 2021; Renko et al., 2018).

However, direct observation of waterspouts in narrow tropical seas remains limited. Tools such as marine weather stations, buoys, and radars are few in number and have a narrow coverage, making it difficult to capture the short duration and small scale of waterspouts (Chan et al., 2020; Chan et al., 2022; Monterde et al., 2025). Even in areas with advanced observation systems, such as Hong Kong and the Pearl River Delta, monitoring the vertical structure of waterspouts remains difficult due to limitations in observation angles and radar beam height above sea level (Chan et al., 2020; Chan et al., 2022). These limitations are even greater in tropical island regions, such as Indonesia, where waterspout reports are usually based only on visual evidence, not detailed meteorological data (Monterde et al., 2025).

Previous research also explains that the mechanism of waterspout formation can vary depending on the type of storm. Many waterspouts appear in non-supercell convective systems, where lower-level rotation is enhanced by surface convergence. Meanwhile, there are also waterspouts associated with supercell storms that have long-lasting mesocyclones (Chan et al., 2020; Chan et al., 2022; Renko et al., 2018). Case studies show that environments conducive to waterspouts are typically characterized by a sufficiently unstable atmosphere, low to moderate wind shear in the lower layers, and strong surface convergence over warm waters. Triggering factors can include weak cold fronts, land-sea wind circulation, or local cyclonic disturbances (Mihajlović et al., 2021; Monterde et al., 2025; Renko et al., 2018). Several instability indices and composite parameters, including the Szilagyi Waterspout Index, have proven to be quite effective in identifying waterspout-prone conditions in semi-

enclosed seas and coastal areas (Renko et al., 2018; Mihajlović et al., 2021).

The development of new-generation geostationary satellites, particularly Himawari-8 and Himawari-9, has greatly aided the monitoring of convective clouds and extreme weather in tropical regions. The Advanced Himawari Imager (AHI) instrument has 16 spectral channels with a spatial resolution of 0.5–2 km and high temporal resolution, namely 10 minutes for full-disk images and 2.5 minutes for regional areas. With this capability, cloud growth can be monitored in detail from its inception to its disappearance (Bessho et al., 2016; Chen et al., 2024). This satellite data is also widely used for operational products such as cloud type identification, cloud top temperature, cloud microstructure, rainfall estimation, and near real-time atmospheric and oceanic information, especially in the South China Sea and surrounding areas that are important for maritime activities (Bessho et al., 2016; Chen et al., 2024; Liu et al., 2024; Zhuge et al., 2024).

However, research that directly combines high-resolution atmospheric reanalysis data with Himawari-8/9 satellite observations to analyze waterspouts in tropical seas is still limited (Chen et al., 2024; Liu et al., 2024; Renko et al., 2018; Zhao et al., 2022). The integration of both datasets is important because satellite imagery can capture the temporal evolution of convective clouds, while reanalysis data provides a three-dimensional representation of atmospheric dynamics and thermodynamic conditions before, during, and after waterspout formation.

The Beliah Strait, located in the Karimun Regency of the Riau Islands, is a narrow maritime passage surrounded by small islands and shallow coastal waters. The region lies within the equatorial maritime continent, which is characterized by persistently warm sea surface temperatures, high atmospheric humidity, and active convective processes throughout the year. In addition, the interaction between local sea–land breeze circulation, complex coastal geometry, and narrow strait topography may enhance low-level convergence and atmospheric instability, creating favorable conditions for localized convective vortices and waterspout development.

On 17 June 2025, a waterspout event was observed in the waters around Nangka Island and Beliah Strait between 11:30 and 13:00 WIB (04:30–06:00 UTC). The phenomenon was widely documented through visual observations and local online news reports from coastal communities in Tanjung Balai Karimun, indicating considerable public attention despite the absence of reported damage. Similar events have also been reported in the surrounding waters in

recent years, suggesting that the local atmospheric and coastal environment may be conducive to recurring waterspout formation.

Therefore, this study aims to analyze the synoptic-to-mesoscale atmospheric conditions associated with the Beliah Strait waterspout event using ERA5 reanalysis data and Himawari-9 satellite imagery. Specifically, this study addresses the following research questions: (1) how did low-level wind convergence and vorticity contribute to the formation of the waterspout; (2) what thermodynamic conditions supported convective initiation and development; and (3) how did convective cloud evolution observed by Himawari-9 relate to the timing and intensification of the event. The results are expected to improve understanding of waterspout formation in narrow tropical seas and support the development of satellite- and reanalysis-based indicators for maritime hazard monitoring and early warning in Indonesian waters.

B. METHOD

This study investigates a waterspout event that occurred on 17 June 2025 over the coastal waters of Karimun Regency, Riau Islands, Indonesia, with particular focus on the Beliah Strait and the surrounding waters of Nangka Island (Figure 1).

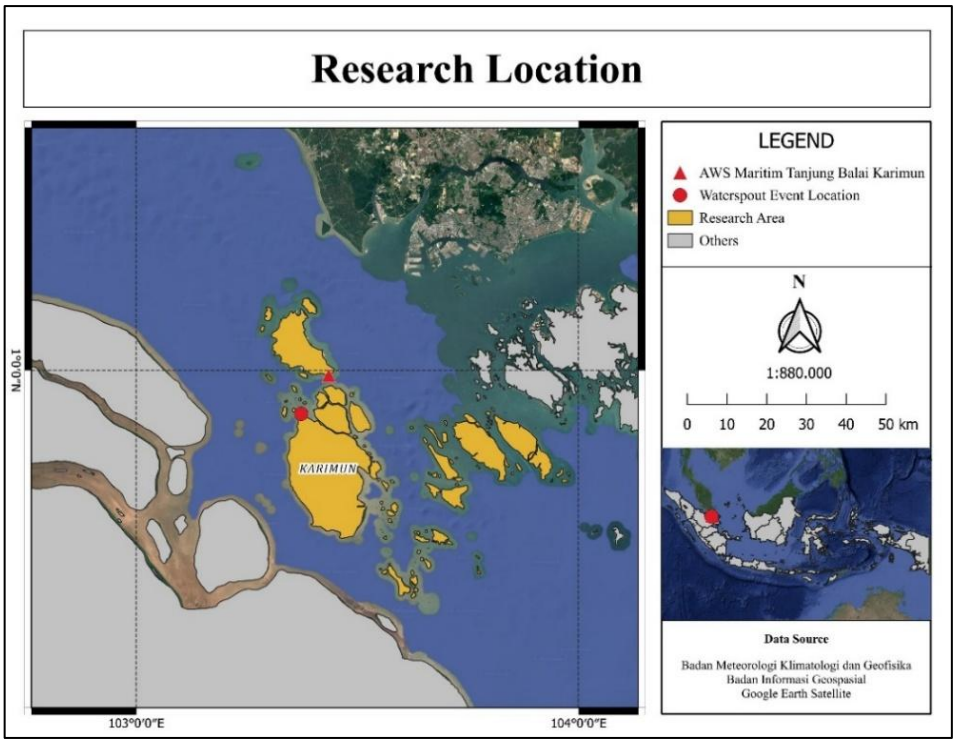

Figure 1. Research Location
(Source: Processed by author, 2026)

The analysis domain extends from 1° S to 3° N and from 101° E to 107° E, encompassing the northern Riau Archipelago and adjacent shallow maritime areas characterized by complex coastal geometry and strong land–sea interactions. The Beliah Strait is located at approximately 0.90° N and 103.37° E and represents a narrow coastal waterway bordered by small islands, where localized atmospheric circulations frequently develop. The waterspout event persisted from approximately 11:30 to 13:00 local time (WIB), with its terminal stage observed near Parit Island.

Surface meteorological conditions were represented using hourly observations from the Maritime Automatic Weather Station (AWS) Digi Tanjung Balai, located approximately 18 km from the event location and serving as the nearest in situ observation. The AWS data include air temperature, surface pressure, and relative humidity, which were processed to produce time series describing the temporal evolution of near-surface thermodynamic conditions before and during the waterspout occurrence. These observations were used to support the interpretation of atmospheric variability at the surface level.

Although the AWS station is located approximately 18 km from the waterspout location, the observations were considered representative of the broader near-surface environmental conditions over the surrounding coastal waters. The AWS data were primarily used to describe temporal variations in temperature, pressure, and relative humidity prior to and during the event, rather than to resolve the microscale vortex structure directly. Due to the localized nature of waterspouts, small-scale convergence and boundary-layer variability near the vortex center may not be fully captured by the station observations. The following is a research flow diagram shown in Figure 2.

Atmospheric reanalysis data were obtained from the European Centre for Medium-Range Weather Forecasts (ECMWF) for 17 June 2025, with a horizontal resolution of 0.125° × 0.125°, and downloaded from the Copernicus Climate Data Store in netCDF format. The selected variables include 10 m wind components (u and v), vertical profiles of relative humidity, vertical vorticity, sea surface temperature (SST), and parameters required for the calculation of atmospheric stability indices. All variables were selected directly during data retrieval and did not require additional diagnostic computation at the download stage. Atmospheric stability was evaluated using several thermodynamic indices, including the K-Index (KI), Total Totals Index (TTI),

Lifted Index (LI), Showalter Index (SI), Convective Available Potential Energy (CAPE), and Convective Inhibition (CIN). The K-Index was calculated as $KI = (T_{850} - T_{500}) + Td_{850} - (T_{700} - Td_{700})$, while the Total Totals Index was defined as $TTI = (T_{850} + Td_{850}) - 2T_{500}$(Galway, 1956; Miller, 1972). The Lifted Index and Showalter Index were derived from the temperature difference between the environment and an adiabatically lifted air parcel at 500 hPa. CAPE and CIN were calculated from parcel buoyancy integration within the atmospheric sounding profile following Doswell and Rasmussen (1994). These indices were derived from ERA5 vertical atmospheric profiles and used to evaluate atmospheric instability, moisture availability, and convective potential associated with the waterspout event.

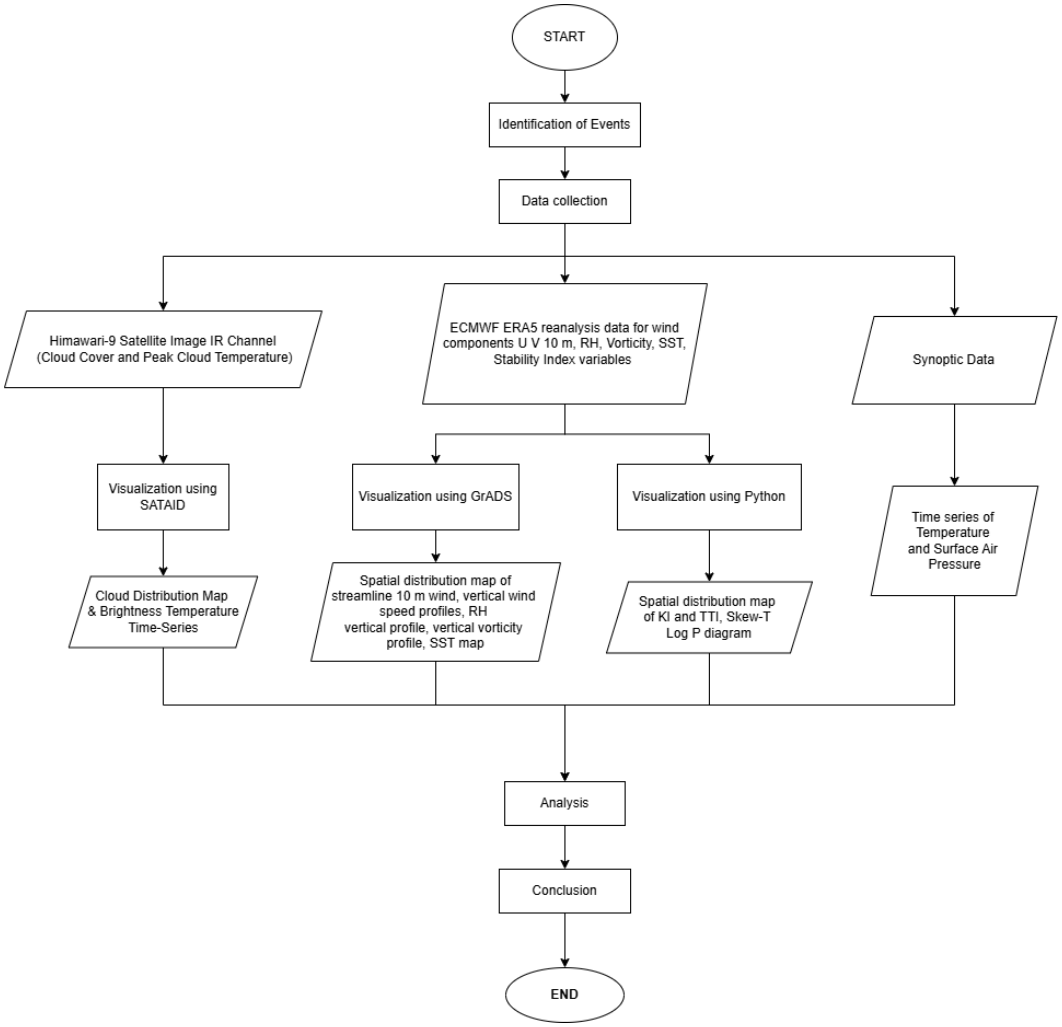

Figure 2. Research Flowchart
(Source: Processed by author, 2026)

The reanalysis data were processed using the Grid Analysis and Display System (GrADS) and Python to generate streamline maps, vertical humidity distributions, SST fields, and atmospheric stability indices, which were used to evaluate the dynamical and thermodynamical environments conducive to convective development and waterspout formation. All reanalysis and satellite data in this study are presented in Coordinated Universal Time (UTC), while Indonesian Western Time (WIB; UTC+7) is additionally provided when necessary for comparison with local observations and eyewitness reports.

Satellite-based cloud analysis was conducted using geostationary observations from Himawari-9. Infrared channel 13 data were acquired in standard satellite observation format and processed using the Satellite Animation and Interactive Diagnosis (SATAID) software. The analysis focused on the visual interpretation of cloud structure and temporal evolution, with particular emphasis on changes in cloud-top brightness temperature as indicators of convective growth and intensification. Temporal tracking of brightness temperature variations was applied to identify the development and maturation of cumulonimbus clouds associated with the waterspout event. The integration of reanalysis, surface observations, and satellite imagery enabled a comprehensive assessment of atmospheric conditions before, during, and after the waterspout occurrence.

C. RESULT AND DISCUSSION

C.1. RESULT

Surface Meteorological Conditions

Surface meteorological conditions during the event were characterized by temporal variations in air temperature, surface pressure, and relative humidity, as summarized in Table 1. To maintain consistency with reanalysis and satellite datasets, all observation times are presented in UTC (WIB = UTC+7). Air temperature increased from 27.9 °C at 02:00 UTC to a maximum of 29.0 °C at 04:00 UTC, then decreased during late morning, reaching 27.1 °C at 07:00 UTC. This evolution reflects surface heating prior to convective growth, followed by cooling associated with cloud development and precipitation.

Surface pressure exhibited a gradual increasing trend throughout the observation period, rising from 1007.4 hPa at 02:00 UTC to 1010.5 hPa at 07:00 UTC. The post-convective pressure increase suggests stabilization of near-surface atmospheric conditions following the mature stage of convection.

Table 1. Hourly Surface Meteorological Parameters Observed at AWS Tanjung Balai during the Waterspout Event on 17 June 2025

Time (UTC)	Temperature (°C)	Pressure (hPa)	Relative Humidity (%)
02:00	27.9	87.3	1007.4
03:00	28.4	85.7	1008.1
04:00	29	83	1008.1
05:00	28.3	88.1	1009.0
06:00	28.3	87	1009.7
07:00	27.1	87.3	1010.5

(Source: Processed by author, 2026)

Relative humidity showed substantial fluctuations during the event period. Values decreased from 87.3% at 02:00 UTC to a minimum of 83.0% at 04:00 UTC, coinciding with peak surface temperature, before increasing sharply to 88.1% at 05:00 UTC and remaining relatively high afterward. The increase in humidity during the convective phase indicates enhanced moisture availability in the lower atmosphere, which supported convective cloud growth and waterspout development.

Low-Level Wind and Surface Convergence

Figure 3 presents the 10-m wind streamlines and surface wind speed distribution at 02:00, 04:00, 05:00, and 06:00 UTC on 17 June 2025. At 02:00 UTC, the low-level wind field was relatively uniform, characterized by weak horizontal gradients and the absence of a distinct convergence zone over the study area.

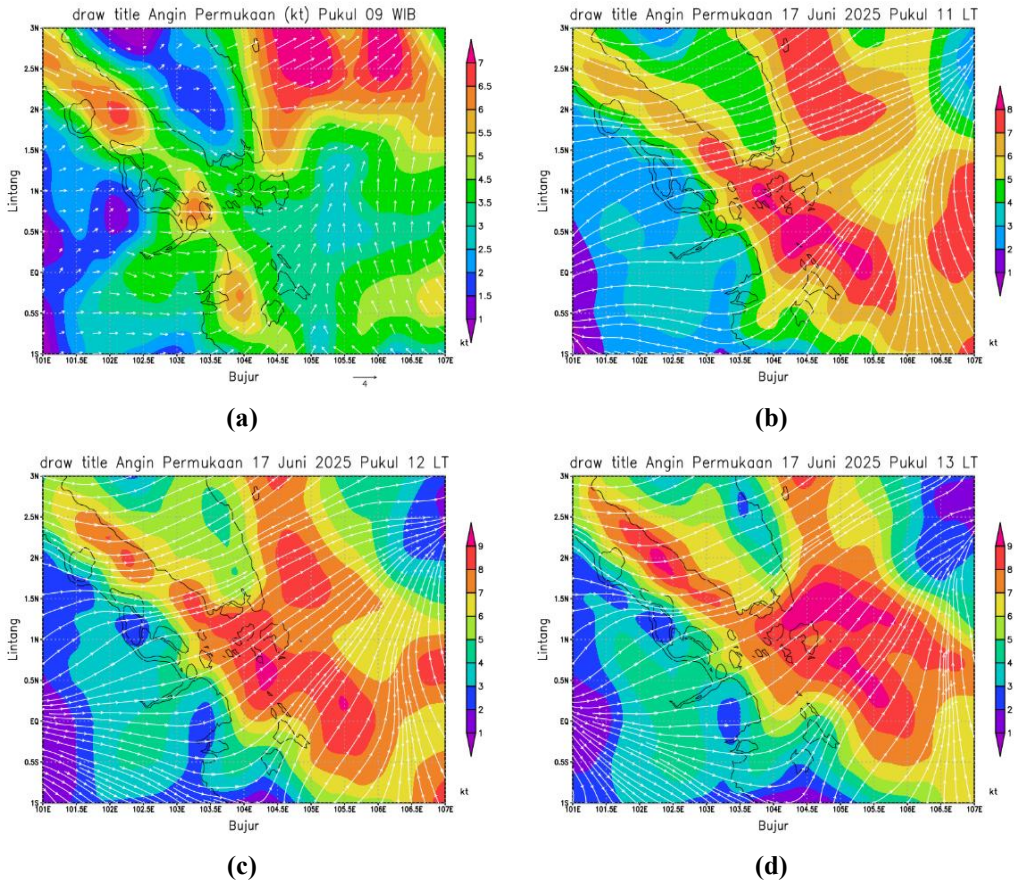

Figure 3. 10-m wind streamlines and surface wind speed from (a) 02:00 UTC, (b) 04:00 UTC, (c) 05:00 UTC, (d) 06:00 UTC
(Source: Processed by author, 2026)

By 04:00 UTC, a surface convergence zone began to develop near Selat Beliah, indicated by

opposing wind directions and increasing streamline density. The convergence intensified further at 05:00 UTC, as shown by tightly packed streamlines and surface wind speeds exceeding 8 kt, suggesting enhanced low-level convergence and localized wind shear near the waterspout location. At 06:00 UTC, the convergence zone weakened, accompanied by reduced wind speeds and a transition toward a more divergent flow pattern across the surrounding waters. The temporal evolution of the low-level wind field indicates that mesoscale surface convergence was strongest during the mature stage of convective development.

Vertical Wind Shear Characteristics

Figure 4 presents the vertical wind speed profiles over Selat Beliah on 17 June 2025 at 05:00 UTC (Figure 4a) and 06:00 UTC (Figure 4b). In Figure 4a, wind speed increased gradually with

height, ranging from less than 2 m s^{-1} near the surface (1000 hPa) to approximately 10 m s^{-1} near 600 hPa. The relatively smooth increase in wind speed indicates weak-to-moderate vertical wind shear within the lower troposphere. In Figure 4b, observed one hour later, the wind profile exhibited a more pronounced increase with altitude, with wind speeds reaching approximately 13–14 m s^{-1} near 550 hPa. The strongest increase occurred between 900 and 700 hPa, where the steeper profile slope suggests enhanced vertical wind shear compared to the earlier period. Above approximately 600 hPa, the wind profile became more uniform, indicating a relatively stable upper-level flow. Overall, the vertical wind shear remained weak to moderate and did not exhibit the strong deep-layer shear typically required for supercell thunderstorm development. This supports the interpretation that the event was a non-supercell waterspout, in which vortex intensification was primarily associated with low-level convergence and vertical stretching of boundary-layer vorticity rather than mesocyclonic rotation.

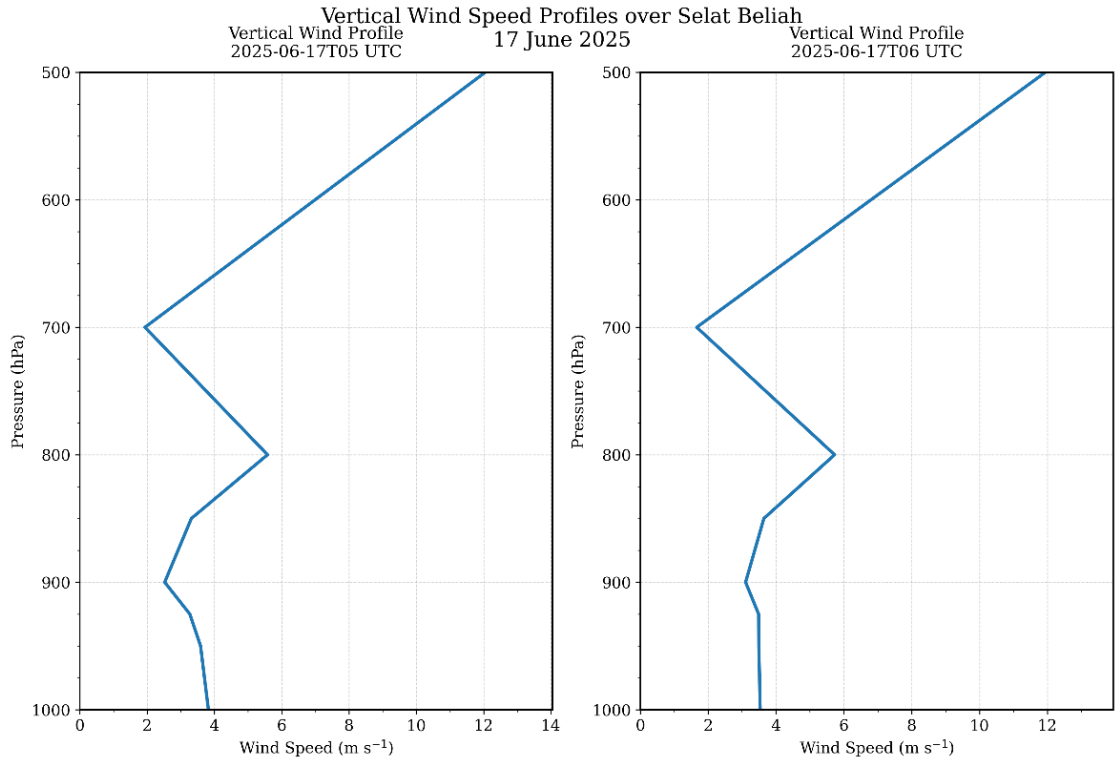

Figure 4. Vertical wind speed profiles over Selat Beliah at (a) 05:00 UTC and (b) 06:00 UTC on 17 June 2025
(Source: Processed by author, 2026)

Thermodynamic Environment

Figure 4a shows the time–height cross-section of relative humidity over Selat Beliah on 17 June 2025. From 00Z to 09Z, the lower troposphere (1000–850 hPa) was characterized by moderate humidity values ranging from 60% to 80%. Beginning at 09Z, a pronounced moistening was observed, with relative humidity exceeding 90% between 950 and 850 hPa. This moist layer persisted and intensified until 12Z, with peak values exceeding 100% near 900 hPa. After 12Z, the depth and magnitude of the moist layer gradually decreased, with relative humidity dropping below 80% by 15Z.

Figure 4b presents the corresponding time–height cross-section of relative vorticity. Between 00Z and 09Z, the vorticity field remained weak and predominantly negative throughout the vertical column. At 09Z, a positive vorticity anomaly emerged near 950 hPa. This anomaly intensified and expanded vertically between 09Z and 12Z, reaching maximum values exceeding 6×10^{-5} s^{-1} around 900 hPa. By 13Z, the anomaly weakened, with reduced magnitude and an upward shift in its vertical structure.

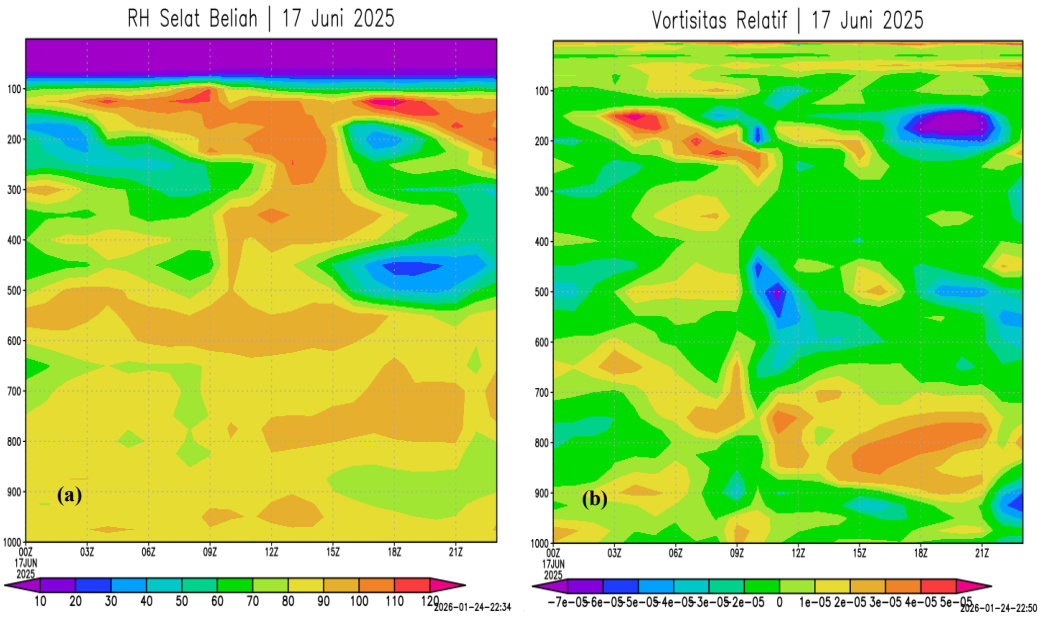

Figure 4. Time–height cross-sections of (a) relative humidity and (b) relative vorticity over Selat Beliah on 17 June 2025
(Source: Processed by author, 2026)

Figure 5a illustrates the spatial distribution of the K-Index at 00 UTC on 17 June 2025, representing an indicator of atmospheric instability. Values across

the study region ranged from approximately 30°C to above 38°C, with the highest concentrations observed over Selat Beliah and its adjacent coastal zones. The relatively uniform spatial pattern, with consistently elevated values across land and sea, suggests the presence of widespread thermodynamic instability extending through the lower and mid-troposphere during the early morning hours. Figure 5b shows the spatial distribution of the Total Totals Index at the same synoptic time, which serves as a proxy for thunderstorm potential. Most areas within the domain exhibited values between 46°C and 52°C, while localized maxima exceeding 54°C were detected near Selat Beliah. These elevated index values were spatially aligned with the K-Index maxima, indicating a thermodynamic environment that was broadly supportive of convective cloud growth and potential thunderstorm initiation.

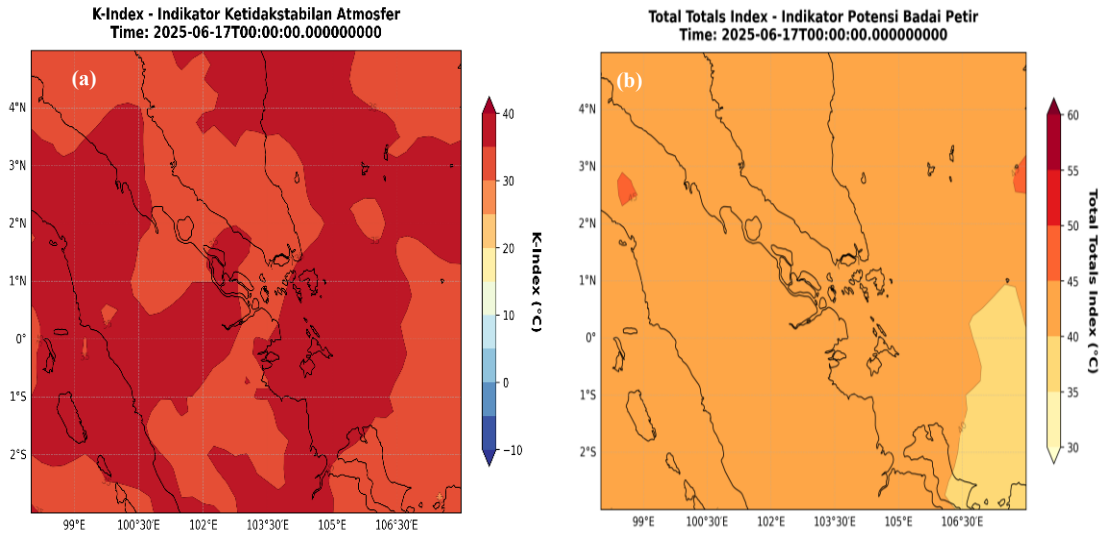

Figure 5. Spatial distribution of (a) K-Index and (b) Total Totals Index at 00 UTC on 17 June 2025.
(Source: Processed by author, 2026)

Figure 6 presents the Skew-T Log-P diagram at 00 UTC on 17 June 2025 for the grid point nearest Selat Beliah (0.90°N, 103.37°E). The lower troposphere was characterized by a moist layer, with the Lifted Condensation Level (LCL) near 952 hPa, indicating a low cloud base favorable for convective initiation. The Level of Free Convection (LFC) was identified at approximately 886 hPa, while the Equilibrium Level (EL) extended up to around 182 hPa, suggesting potential for deep vertical cloud development.

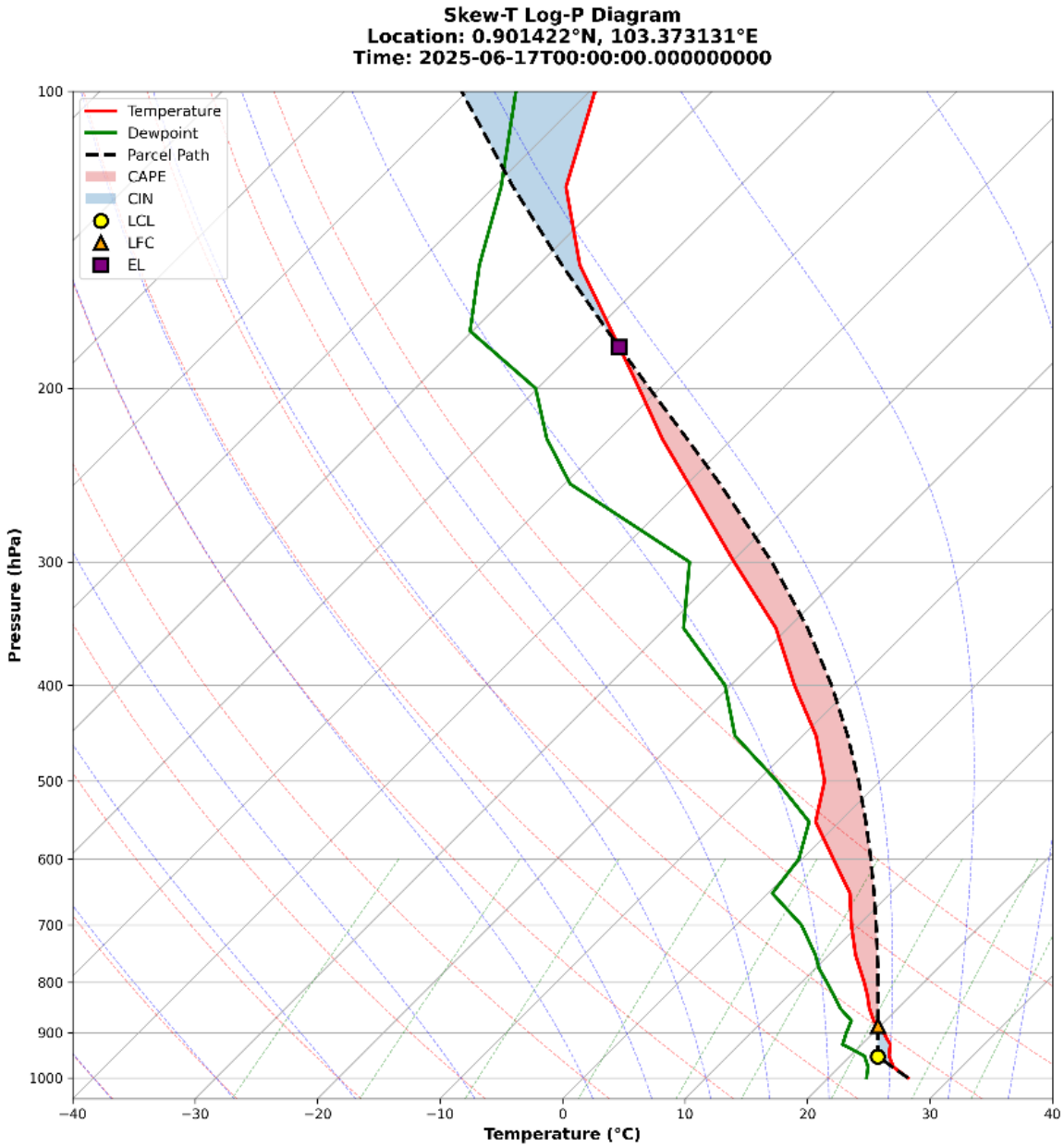

Figure 6. Skew-T Log-P diagram over Selat Beliah (0.90°N, 103.37°E) at 00 UTC on 17 June 2025.
(Source: Processed by author, 2026)

The calculated CAPE value of 1204.3 J kg^{-1} indicates moderate convective instability, supported by weak convective inhibition (CIN = −9.9 J kg^{-1}), allowing parcels to ascend with minimal resistance. The negative Lifted Index (−2.77°C) further confirms atmospheric instability, despite the positive Showalter Index, which suggests convection was primarily driven by low-level forcing

rather than mid-tropospheric instability. These thermodynamic conditions preceded the observed increase in low-level convergence and convective cloud development identified between 04:00 and 06:00 UTC (11:00–13:00 WIB). Overall, the thermodynamic profile was conducive to deep convection when combined with mesoscale convergence and moisture availability.

Sea Surface Temperature

Figure 7 presents the spatial distribution of Sea Surface Temperature (SST) across the western Pacific and Southeast Asian region on 17 June 2025. SST values ranged from approximately 27.0°C to above 30.5°C, with the warmest waters observed in the equatorial zone near the Riau Islands and northern Sumatra.

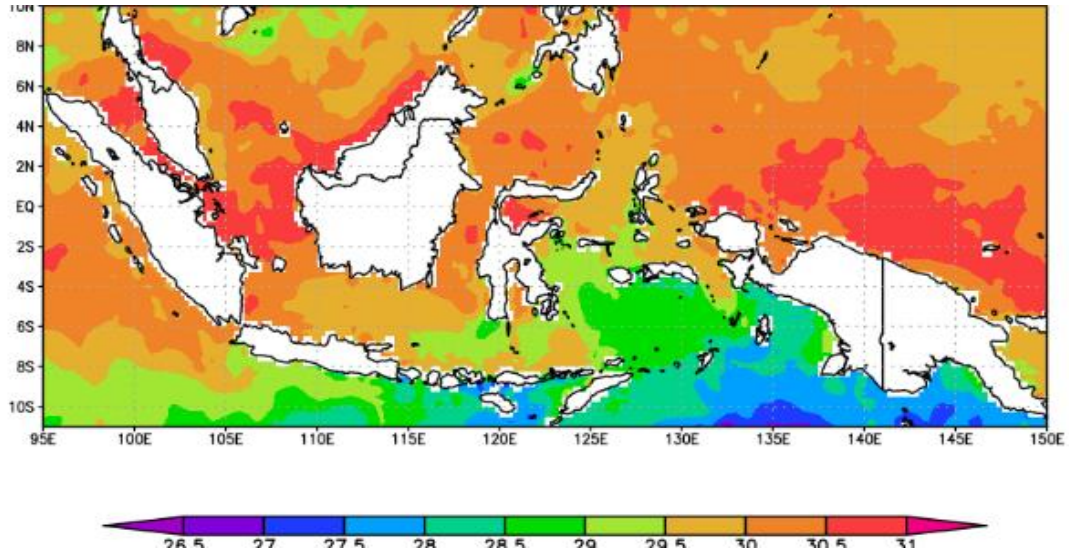

Figure 7. Sea Surface Temperature (SST) Distribution Map
(Source: Processed by author, 2026)

The temperature gradient was relatively smooth, with broad areas exceeding 29.5°C extending from the southern South China Sea to the Java Sea. Localized maxima above 30°C were evident near Selat Beliah, indicating a warm ocean surface condition over the convective source region. Cooler SST values below 28°C were confined to higher latitudes and offshore areas east of the Philippines.

Convective Cloud Characteristics from Himawari-9

Figure 8 presents a sequence of infrared satellite images from Himawari-9 on 17 June 2025 at 04:00, 05:00, and 06:00 UTC. At 04:00 UTC, a convective cloud cluster was observed over Selat Beliah and surrounding waters, characterized by cold cloud tops with brightness temperatures below −70°C, indicated by deep red and

orange shades. By 05:00 UTC, the convective system expanded spatially, with increased coverage of cold cloud tops and enhanced vertical development. At 06:00 UTC, the cloud structure remained organized, with persistent cold cloud tops and dense cloud mass concentrated over the same region. The temporal evolution suggests sustained deep convection over the area during the early morning hours.

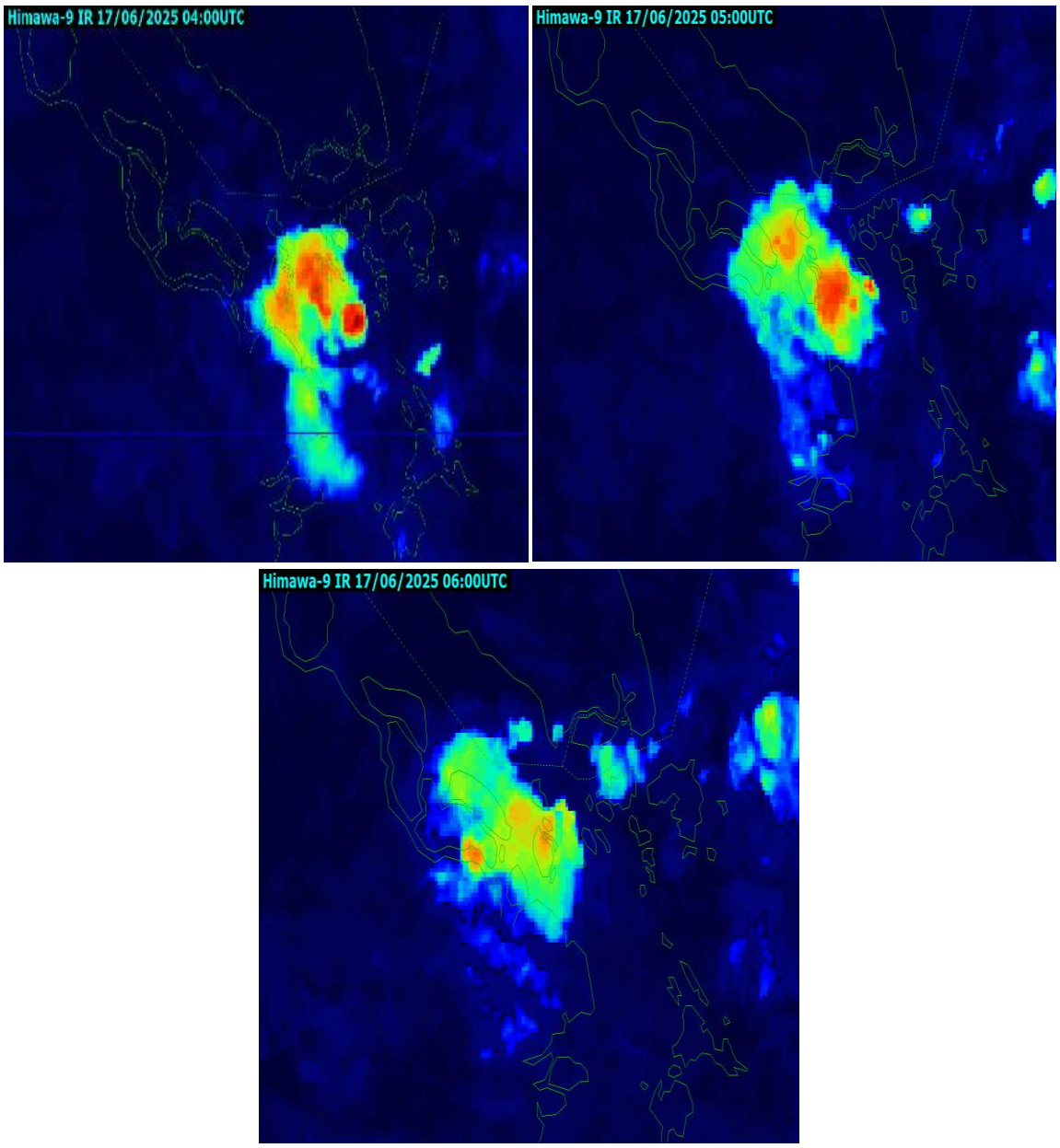

Figure 8. Cloud-top Brightness Temperature Map, Band 13
(Source: Processed by author, 2026)

Figure 9 shows the time series of cloud-top brightness temperature over Selat Beliah on 17 June 2025 between 03:00 and 07:00 UTC. Consistent with the Himawari-9 infrared imagery shown in Figure 8, brightness temperature decreased rapidly beginning around 03:00 UTC, reaching values below −60°C, which indicates the rapid vertical growth of deep convective clouds and the development of very cold cloud tops.

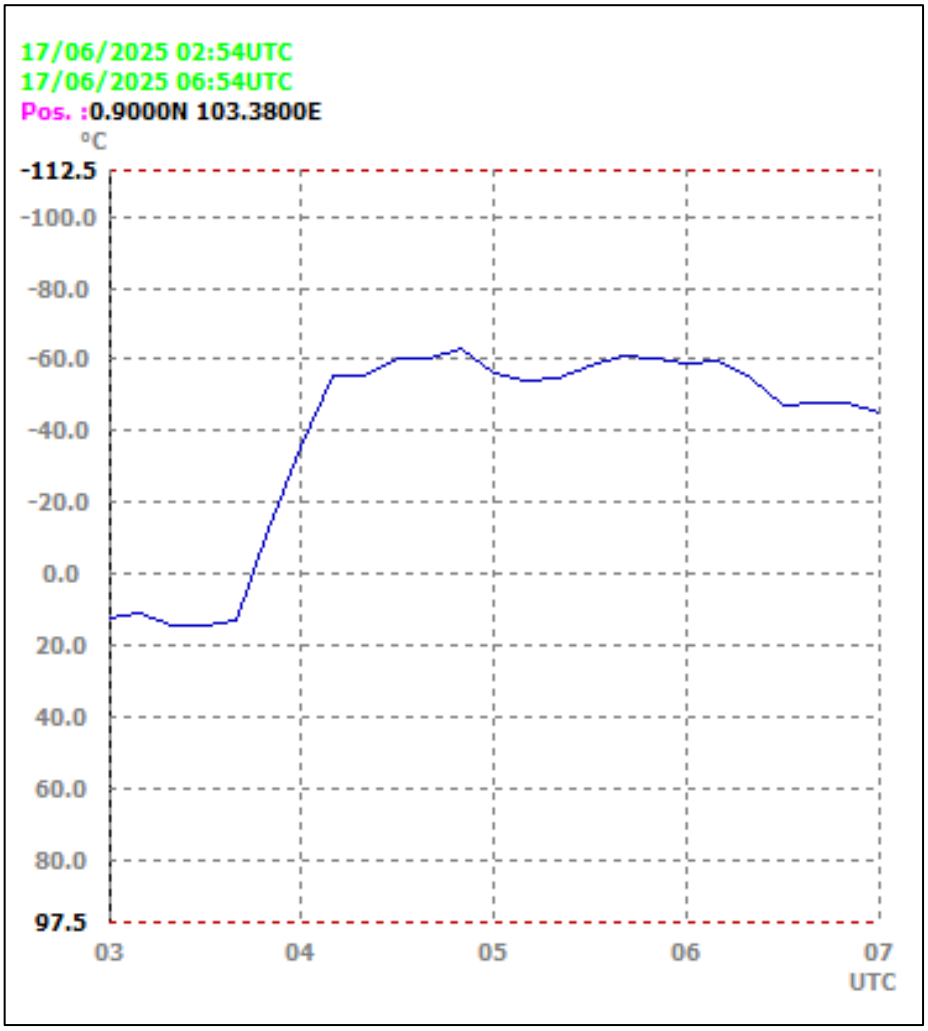

Figure 9. Time series of cloud-top brightness temperature over Selat Beliah from 03:00 to 07:00 UTC on 17 June 2025
(Source: Processed by author, 2026)

Between 03:30 and 06:00 UTC, brightness temperatures remained persistently low, fluctuating primarily between −60°C and −40°C, suggesting sustained deep convection over the study area. The coldest cloud-top temperatures occurred near the mature stage of the convective system, temporally coinciding

with the period of strongest low-level convergence and enhanced positive vorticity identified in Figures 3 and 4b. After 06:00 UTC, brightness temperatures gradually increased toward approximately −40°C by 07:00 UTC, indicating weakening convective intensity and a gradual reduction in cloud-top height. Overall, the brightness temperature evolution quantitatively confirms the growth, persistence, and subsequent weakening of the convective system associated with the waterspout event.

C.2. DISCUSSION

Synoptic–Mesoscale Setting Supporting Waterspout Formation

On June 17, 2025, atmospheric conditions showed several factors often associated with waterspout formation. The atmospheric environment at that time was quite unstable, with high humidity in the lower to middle troposphere and positive vorticity in the lower layers. Similar patterns have also been widely reported in semi-enclosed coastal areas such as the Adriatic Sea and the coast of Montenegro, where waterspouts frequently occur (Mihajlović et al., 2021; Sioutas & Keul, 2007; Renko et al., 2013; Renko et al., 2016; Renko et al., 2018). In these areas, waterspouts usually form not because of strong large-scale forcing, but are more predominantly triggered by local convergence and moist air over warm seas.

As a narrow sea lane, the Beliah Strait likely plays a role similar to that of bays or straits in the Adriatic region. Previous studies have shown that this type of coastal geography can concentrate lower-level winds and strengthen convergence, thereby supporting the formation of vortices in coastal or semi-enclosed waters (Mihajlović et al., 2021; Sioutas & Keul, 2007; Renko et al., 2013; Renko et al., 2016). Thus, the event in the Beliah Strait is consistent with the concept that large-scale atmospheric instability can be amplified by local factors at the mesoscale.

Role of Low-Level Wind Convergence and Vorticity Intensification

Before the waterspout formed, the analysis showed an increase in low-level wind convergence near the surface (10 m), accompanied by the strengthening of positive vorticity over Selat Beliah. The convergence zone became more organized between 04:00 and 05:00 UTC, coinciding with the period of maximum convective development observed in the Himawari-9 imagery. Similar patterns have been reported in previous waterspout studies, where localized surface convergence acts as a key mechanism for vortex intensification in coastal and semi-enclosed seas (Mihajlović et al., 2021; Renko et al., 2013; Renko et al., 2018; Sioutas & Keul, 2007).

The vertical wind profile derived from ERA5 also indicated relatively weak to moderate vertical wind shear through the lower troposphere. Wind speed increased gradually with height, without evidence of strong directional shear or intense upper-level jet influence. The strongest increase in wind speed occurred between 900 and 700 hPa, while the upper layer remained comparatively stable. These characteristics are consistent with environments favorable for non-supercell waterspouts, which typically develop under weak synoptic forcing and modest vertical shear conditions rather than within organized supercell thunderstorms (Renko et al., 2018; Sioutas & Keul, 2007).

This process is consistent with the conceptual model of non-supercell waterspouts, in which pre-existing low-level vorticity along convergence boundaries is stretched vertically by convective updrafts. In such cases, vortex formation is controlled primarily by mesoscale convergence and boundary-layer dynamics instead of persistent mesocyclonic rotation (Renko et al., 2016; Renko et al., 2018; Sioutas & Keul, 2007). Therefore, the Beliah Strait event can be classified as a non-supercell waterspout, with local convergence, low-level vorticity enhancement, and moderate vertical wind shear playing dominant roles in its development.

Thermodynamic Conditions and Convective Instability

The thermodynamic conditions during the event were favorable for convective development in a tropical maritime environment. The atmosphere was characterized by moderate instability, high lower-tropospheric humidity, weak convective inhibition (CIN), and a relatively low Lifted Condensation Level (LCL). A CAPE value of approximately 1200 J kg^{-1} indicates sufficient buoyant energy to support deep convection once lifting mechanisms were present, while the weak CIN allowed air parcels to ascend with minimal resistance. In addition, the negative Lifted Index confirms the presence of conditional atmospheric instability associated with active convection.

Although the Showalter Index remained positive, this does not necessarily indicate the absence of convection in tropical environments. The Showalter Index is derived from an air parcel lifted from 850 hPa and is therefore less sensitive to near-surface moisture accumulation and boundary-layer instability, which are dominant features in tropical maritime convection. In contrast, the Lifted Index incorporates surface-based thermodynamic conditions and is more representative of convection triggered by low-level moisture convergence and surface heating. Consequently, the negative Lifted Index, together with moderate CAPE, weak CIN,

and a low LCL, provides stronger evidence of a favorable convective environment over Selat Beliah.

Similar combinations of moderate CAPE, weak inhibition, high humidity, and low cloud-base height have been widely reported in studies of waterspouts and tropical thunderstorms in the Mediterranean, India, and Sri Lanka, where convection is frequently initiated by mesoscale convergence rather than strong upper-level forcing (Fernando et al., 2021; Jayakrishnan & Babu, 2014; Matthew et al., 2021; Mihajlović et al., 2021; Renko et al., 2013; Renko et al., 2018; Sioutas & Keul, 2007; Suresh & Bhatnagar, 2022). Overall, the thermodynamic structure observed over the Beliah Strait was consistent with an environment conducive to non-supercell waterspout formation.

Influence of Sea Surface Temperature and Air–Sea Interaction

Sea surface temperatures around the Beliah Strait are warm and relatively uniform. This is consistent with previous findings that warm oceans provide heat and moisture energy to support deep convection in tropical and subtropical regions (Mihajlović et al., 2021; Raymond & Fuchs-Stone, 2020; Rogers et al., 2020; Sioutas & Keul, 2007). Studies in the Mediterranean also show that warm SST in summer is often associated with moist and unstable lower layers (Renko et al., 2016; Renko et al., 2018; Sioutas & Keul, 2007).

Even in the absence of a strong horizontal SST gradient, small temperature differences between land and sea can still enhance land-sea wind circulation. Similar effects have also been reported in studies of coastal convection in India and Sri Lanka (Fernando et al., 2021; Jayakrishnan & Babu, 2014; Suresh & Bhatnagar, 2022). This process likely helps maintain lower layer moisture supply and mesoscale convergence in these narrow straits.

Convective Cloud Evolution Observed by Himawari-9

Himawari-9 infrared imagery showed the evolution of convection from an initially developing cloud cluster into a mature deep convective system over Selat Beliah. The satellite observations indicated progressive cloud-top cooling between 04:00 and 06:00 UTC, accompanied by an expansion of cold cloud coverage over the study area. Cloud-top brightness temperatures below −70°C during the mature stage suggest the presence of deep cumulonimbus clouds with strong vertical development. Similar cloud-top cooling signatures have been widely associated with vigorous tropical convection and intense updraft activity in previous satellite-based studies (Fernando et al., 2021; Raymond & Fuchs-Stone, 2020; Rogers et al., 2020; Umakanth et al., 2020).

The brightness temperature time series further showed a rapid decrease beginning around 03:00 UTC, followed by

persistently cold cloud-top temperatures between approximately 03:30 and 06:00 UTC. This prolonged period of low brightness temperature indicates sustained deep convection over Selat Beliah. After 06:00 UTC, brightness temperatures gradually increased, suggesting weakening convective intensity and warming cloud tops associated with the dissipating stage of the convective system.

The timing of the coldest cloud-top temperatures corresponded closely with the period of strongest low-level convergence and enhanced positive vorticity identified in the ERA5 analysis. This temporal relationship suggests that mesoscale convergence and boundary-layer vorticity played important roles in maintaining deep convective updrafts during the waterspout event. Although satellite-based waterspout studies in the Asia–Pacific region remain limited, the observed cloud evolution and cloud-top cooling patterns are consistent with characteristics commonly documented in tropical mesoscale convective systems and severe maritime convection.

Implications for Waterspout Monitoring and Early Warning in Indonesian Waters

The integration of high-resolution Himawari-9 satellite data with atmospheric reanalysis shows great potential for waterspout monitoring in Indonesian waters, where observational data is still scarce. A similar approach has been successfully applied in the Adriatic region to assess the waterspout environment and support the use of the Szilagyi Waterspout Index (Renko et al., 2013; Renko et al., 2018; Sioutas & Keul, 2007).

Given the limitations of marine radar and in situ observations, combining satellite-based indicators of cloud development with reanalysis data on convergence and instability could serve as an early warning signal for waterspout risk. This approach is in line with severe convection nowcasting methods in other tropical regions, which utilize instability indices and lightning observations (Fernando et al., 2021; Suresh & Bhatnagar, 2022; Yavuz, 2024). From an operational perspective, this integration can improve maritime hazard warnings in busy shipping lanes, as waterspouts, despite being short-lived, remain a risk to small vessels and coastal infrastructure (Mihajlović et al., 2021; Renko et al., 2016).

Limitations and Future Research Directions

Although the analysis results indicate atmospheric conditions conducive to waterspout formation in the Beliah Strait, there are several limitations that should be noted. First, the use of reanalysis data has limited spatial and temporal resolution, so that small details of convergence and vorticity structures may

not be fully detected (Mihajlović et al., 2021; Renko et al., 2013; Renko et al., 2018; Sherburn & Parker, 2019). Second, the lack of marine radar and in situ observations makes direct validation of the intensity and structure of the vortex difficult. This is common in waterspout studies, which rely more on visual reports and infrequent sounding data (Renko et al., 2016; Sioutas & Keul, 2007).

For future research, analysis should be expanded to examine several other waterspout events so that general patterns can be more clearly identified. In addition, combining reanalysis data with high-resolution regional models can help capture more accurate mesoscale details. Additional observations such as ship data, coastal radar, wind profilers, and high-resolution satellite products are also important to strengthen the analysis. These recommendations are in line with recent studies on tropical convection and extreme weather in tropical and subtropical regions (Fernando et al., 2021; Guo et al., 2023; Jayakrishnan & Babu, 2014; Matthew et al., 2021; Raymond & Fuchs-Stone, 2020; Suresh & Bhatnagar, 2022; Yavuz, 2024).

D. CONCLUSION

This study demonstrates that the waterspout event over the Beliah Strait on 17 June 2025 resulted from the interaction between thermodynamic instability, high lower-tropospheric humidity, and mesoscale dynamical processes. Reanalysis data indicate a moderately unstable atmosphere, characterized by CAPE of 1204.3 J kg^{-1}, weak CIN, and a low LCL near 952 hPa, supporting favorable conditions for convective initiation. Although the Showalter Index suggested limited mid-level instability, the negative Lifted Index and high parcel buoyancy up to an equilibrium level near 182 hPa confirmed the potential for deep convection under sufficient low-level forcing.

Enhanced surface wind convergence, increasing boundary-layer vorticity, and weak-to-moderate vertical wind shear supported the classification of the event as a non-supercell waterspout. Himawari-9 observations further revealed rapid convective cloud growth and sustained cold cloud-top temperatures concurrent with peak convergence and vorticity intensification. Overall, the integration of reanalysis data and geostationary satellite observations proved effective for identifying atmospheric conditions conducive to waterspout formation in tropical maritime regions with limited observations. Nevertheless, this study remains limited by the spatial resolution of reanalysis data and the absence of direct radar or in situ vortex observations. Future studies should include validation using independent observational datasets and extend the analysis to additional waterspout events across Indonesian waters.

BIBLIOGRAPHY

Bessho, K., Date, K., Hayashi, M., Ikeda, A., Imai, T., Inoue, H., Kumagai, Y., Miyakawa, T., Murata, H., Ohno, T., Okuyama, A., Oyama, R., Sasaki, Y., Shimazu, Y., Shimoji, K., Sumida, Y., Suzuki, M., Taniguchi, H., Tsuchiyama, H., Uesawa, D., Yokota, H., & Yoshida, R. (2016). An Introduction to Himawari-8/9—Japan's New-Generation Geostationary Meteorological Satellites. Journal of the Meteorological Society of Japan, 94, 151-183. https://doi.org/10.2151/jmsj.2016-009

Chan, P., Kong, W., Wurman, J., Kosiba, K., Robinson, P., Zhan, T., Lok, C., & Li, Q. (2022). Observational analysis of a waterspout sighted in Macao, China, on 1 June 2021. Weather, 78. https://doi.org/10.1002/wea.4296

Chan, P., Tse, S., Lee, J., & Li, Q. (2020). Analysis of a waterspout at Zhuhai, China, on June 12, 2019. *Meteorological Applications*, *27*. https://doi.org/10.1002/met.1904

Chen, X., Letu, H., Shang, H., Ri, X., Tang, C., Ji, D., Shi, C., & Teng, Y. (2024). Rainfall Area Identification Algorithm Based on Himawari-8 Satellite Data and Analysis of its Spatiotemporal Characteristics. Remote. Sens., 16, 747. https://doi.org/10.3390/rs16050747

Doswell, C., & Rasmussen, E. (1994). The Effect of Neglecting the Virtual Temperature Correction on CAPE Calculations. Weather and Forecasting, 9, 625–629. https://doi.org/10.1175/1520-0434(1994)009<0625:TEONTV>2.0.CO;2

Fernando, M., Millangoda, M., & Premalal, S. (2021). Analyze and comparison of the atmospheric instability using K-index, lifted index, total totals index, convective available potential energy (CAPE), and convective inhibition (CIN) in development of thunderstorms in Sri Lanka during second inter-monsoon. *Multi-Hazard Early Warning and Disaster Risks*. https://doi.org/10.1007/978-3-030-73003-1_41

Galway, J. (1956). The Lifted Index as a Predictor of Latent Instability. Bulletin of the American Meteorological Society, 37, 528–529. https://doi.org/10.1175/1520-0477-37.10.528

Guo, X., Guo, J., Zhang, D., & Yun, Y. (2023). Vertical divergence profiles as detected by two wind-profiler mesonets over East China: Implications for nowcasting convective storms. *Quarterly Journal of the Royal Meteorological Society*, *149*, 1629–1649. https://doi.org/10.1002/qj.4474

Jayakrishnan, P., & Babu, C. (2014). Assessment of convective activity using stability indices as inferred from radiosonde and MODIS data. *Applied Categorical Structures*, 2014, 122–130. https://doi.org/10.4236/acs.2014.41014

Liu, J., Yu, J., Lin, C., He, M., Liu, H., Wang, W., & Min, M. (2024). Near-real-time atmospheric and oceanic

science products of Himawari-8 and Himawari-9 geostationary satellites over the South China Sea. Earth System Science Data. https://doi.org/10.5194/essd-16-4949-2024

Matthew, O., Abiye, O., & Ayoola, M. (2021). Assessment of static stability indices and related thermodynamic parameters for predictions of atmospheric convective potential and precipitation over Nigeria. *Meteorology and Atmospheric Physics*, 1–17. https://doi.org/10.1007/s00703-020-00772-z

Mihajlović, J., Burić, D., & Milenković, M. (2021). Synoptic characteristics of an extreme weather event: The tornadic waterspout in Tivat (Montenegro), on June 9, 2018. *Geographica Pannonica*, *94*, 68–90. https://doi.org/10.7163/gpol.0194

Miller, R. (1972). Notes on Analysis and Severe-Storm Forecasting Procedures of the Air Force Global Weather Central. Air Weather Service Technical Report, Air Force Global Weather Central.

Monterde, D., Carbajal, N., León-Cruz, J., & Pineda-Martínez, L. (2025). Climatology of waterspouts in Mexico and numerical modeling of a particular case. *Environmental Research Communications*, *7*. https://doi.org/10.1088/2515-7620/adb095

Raymond, D. J., & Fuchs-Stone, Ž. (2020). Emergent properties of convection in OTREC and PREDICT. *Journal of Geophysical Research: Atmospheres*, *126*. https://doi.org/10.1029/2020JD033585

Renko, T., Ivušić, S., Prtenjak, T., Šoljan, V., & Horvat, I. (2018). Waterspout forecasting method over the Eastern Adriatic using a high-resolution numerical weather model. *Pure and Applied Geophysics*, *175*, 3759–3778. https://doi.org/10.1007/s00024-018-1833-x

Renko, T., Kozarić, T., & Tudor, M. (2013). An assessment of waterspout occurrence in the Eastern Adriatic basin in 2010: Synoptic and mesoscale environment and forecasting method. *Atmospheric Research*, *123*, 71–81. https://doi.org/10.1016/j.atmosres.2012.06.018

Renko, T., Kuzmić, J., Šoljan, V., & Mahović, N. (2016). Waterspouts in the Eastern Adriatic from 2001 to 2013. *Natural Hazards*, *82*, 441–470. https://doi.org/10.1007/s11069-016-2192-5

Rogers, R., Reasor, P., Zawislak, J., & Nguyen, L. (2020). Precipitation processes and vortex alignment during the intensification of a weak tropical cyclone in moderate vertical shear. *Monthly Weather Review*. https://doi.org/10.1175/MWR-D-19-0315.1

Sherburn, K., & Parker, M. (2019). The development of severe vortices within simulated high-shear, low-CAPE convection. *Monthly Weather Review*. https://doi.org/10.1175/MWR-D-18-0246.1

Sioutas, M., & Keul, A. (2007). Waterspouts of the Adriatic, Ionian and Aegean Sea and their meteorological environment. *Atmospheric Research*, *83*, 542–557. https://doi.org/10.1016/j.atmosres.2005.08.009

Suresh, R., & Bhatnagar, A. (2022). Pre-convective environment of pre-monsoon thunderstorms around Chennai – A thermodynamical study. *MAUSAM*. https://doi.org/10.54302/mausam.v56i3.996

Umakanth, N., Satyanarayana, G., Simon, B., & Rao, M. (2020). Satellite-based interpretation of stability parameters on convective systems over India and Sri Lanka. *Asian Journal of Atmospheric Environment*, *14*, 119–132. https://doi.org/10.5572/ajae.2020.14.2.119

Yavuz, V. (2024). Performance analyses of thermodynamic indices and atmospheric parameters in thunderstorm and non-thunderstorm days in Istanbul, Turkey. *Pure and Applied Geophysics*, *181*, 2297–2316. https://doi.org/10.1007/s00024-024-03521-0

Zhao, Y., Liu, C., Di, D., & Tang, S. (2022). High-resolution typhoon precipitation integrations using satellite infrared observations and multisource data. *Atmospheric Measurement Techniques*, *15*, 2791–2806. https://doi.org/10.5194/amt-15-2791-2022

Zhuge, X., Zou, X., Yu, L., Li, X., Zeng, M., Chen, Y., Zhang, B., Yao, B., Tang, F., Chen, F., & Kan, W. (2024). Introduction to the NJIAS Himawari-8/9 cloud feature dataset for climate and typhoon research. *Earth System Science Data*, *16*, 1747–1762. https://doi.org/10.5194/essd-16-1747-2024